Electronic states in magnetic nanostructures

by F. J. Himpsel T. A. Jung P. F. Seidler

This paper provides a survey of electronic states in magnetic nanostructures, how they differ from bulk states, and how these changes are related to interesting magnetic phenomena such as oscillatory coupling and giant magnetoresistance (GMR). After explaining the role of quantum well states and spindependent electron reflectivity in magnetic multilayers, we turn our attention to lowerdimensional structures such as stripes and dots. Fabrication methods are described that use a stepped surface as template. For monitoring the growth mode, it is critical to distinguish and identify different metals at a surface by scanning tunneling microscopy (STM). This is achieved via resonant tunneling through metal-specific surface and image states.

Why nanostructures?

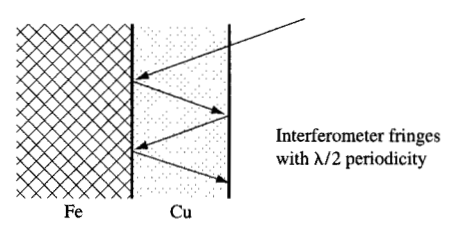
The popularity of the affix *nano* begs the question why the physics and technology of nanostructures should be special. Are there phenomena occurring at the nanometer scale that are not encountered in the more familiar microworld? A rather global answer concentrates on two related phenomena: 1) Nanometer dimensions are comparable to the electron wavelength in a solid. 2) When electrons are confined to dimensions comparable to their wavelength, the continuum of bulk energy bands becomes quantized into discrete quantum well states.

The energy spacings of the states increase as the structures become smaller, eventually becoming greater than the thermal energy kT. If that happens for states at the Fermi level $E_{\rm F}$, only a single quantum level is accessible thermally. Consequently, the dimensionality of electrons is reduced in a nanostructure because they cannot propagate along the directions of the confinement. These effects can be illustrated by analyzing the electronic states in thin metal overlayers by photoemission and its time-reversed counterpart, inverse photoemission. The two techniques are particularly useful for probing electronic states, since they make it possible to determine the complete set of quantum numbers that characterize an electron in a crystal, i.e., energy E, momentum \mathbf{p} (or wave vector $\mathbf{k} = \mathbf{p}/\hbar$), angular symmetry, and spin. Photoemission measures occupied states, inverse photoemission unoccupied states. We focus on electronic states near the Fermi level which are essential in transport properties, such as magnetoresistance, and drive magnetic transitions. For a recent review of magnetic nanostructures, see [1].

The density of unoccupied states at $E_{\rm F}$ with parallel momentum ${\bf k}^{\parallel}=0$ is displayed in **Figure 1** for Cu films grown epitaxially on an fcc Fe film which, in turn, was grown epitaxially on a Cu(100) single crystal [2]. As the thickness of the Cu overlayer is increased, the density of states oscillates with a period of about six atomic layers (about 1 nm), which brings us into the nanometer regime. The amplitude of the oscillations is significant—there is no zero offset in Figure 1. In fact, the amplitude appears to be limited by the smoothness of the interfaces that is achievable by current growth techniques. The smoother

^oCopyright 1998 by International Business Machines Corporation. Copying in printed form for private use is permitted without payment of royalty provided that (1) each reproduction is done without alteration and (2) the *Journal* reference and IBM copyright notice are included on the first page. The title and abstract, but no other portions, of this paper may be copied or distributed royalty free without further permission by computer-based and other information-service systems. Permission to *republish* any other portion of this paper must be obtained from the Editor.

0018-8646/98/\$5.00 © 1998 IBM



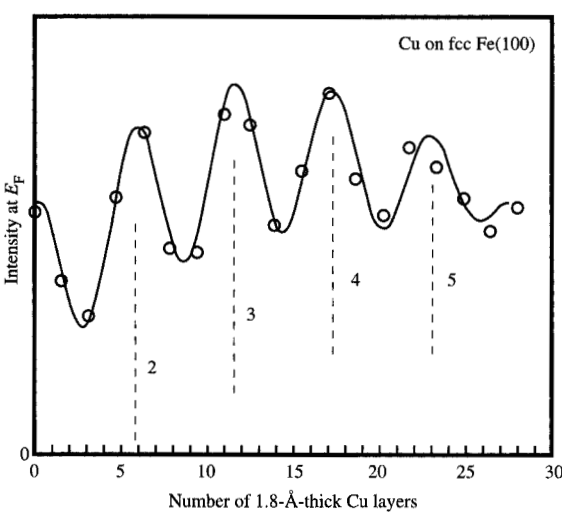


Figure 1

Oscillations in the density of states versus thickness for Cu grown epitaxially on an fcc Fe film which was grown epitaxially on a Cu(100) single crystal. A simple interferometer model explains the oscillations as interference fringes of electron waves reflected back and forth at the interfaces. This allows a direct measurement of the wavelength of the envelope wave function. From [2, 4], reproduced with permission.

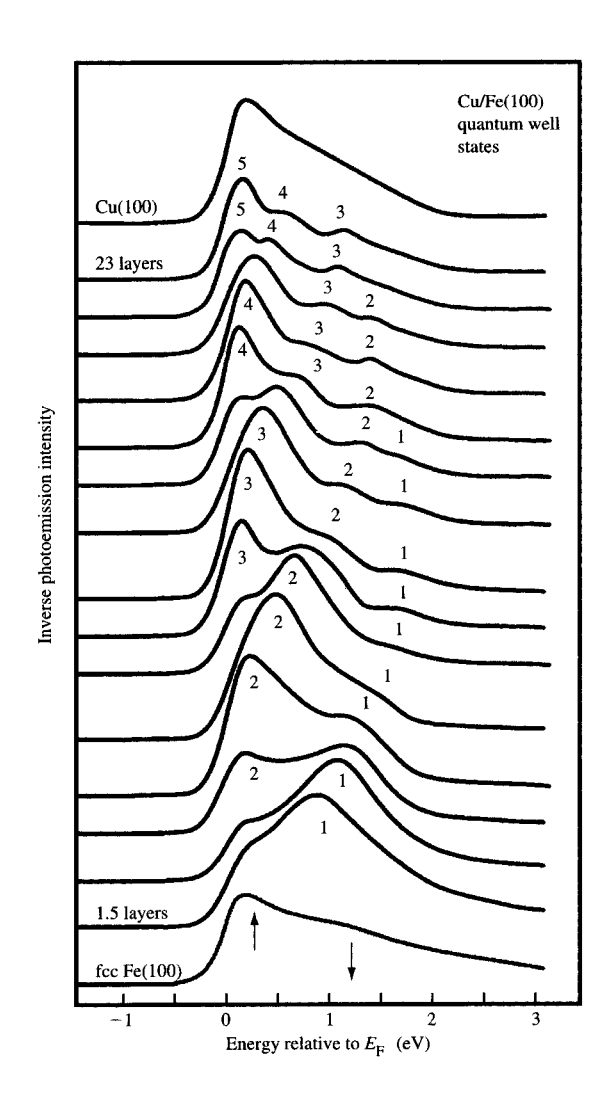
the films, the larger the amplitude [3]. This explains why such oscillations have been difficult to observe in thin films so far.

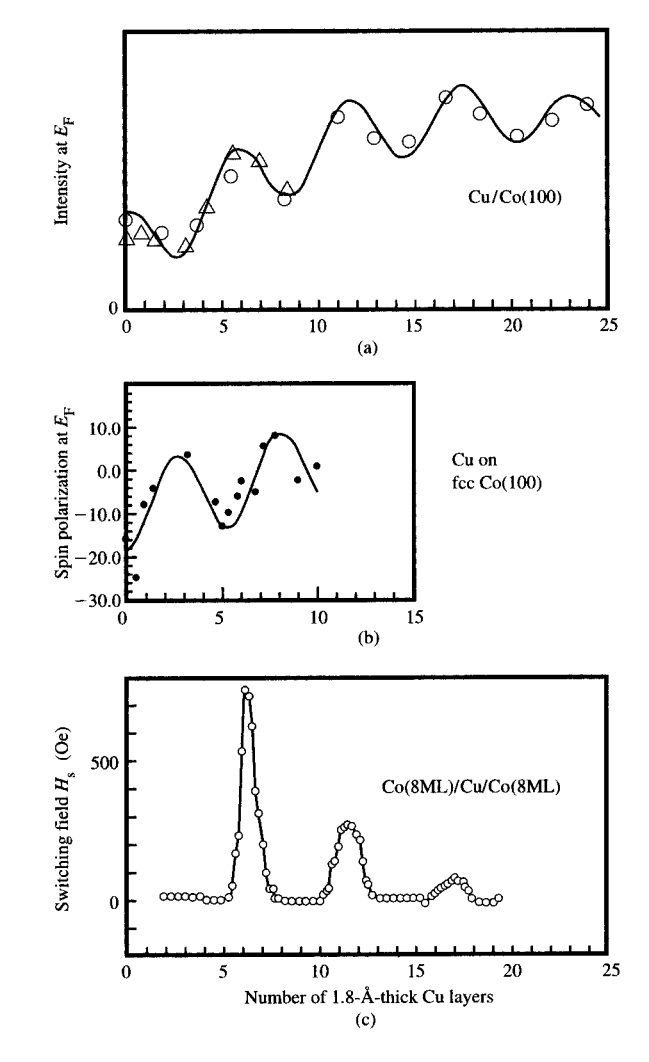
The density-of-states oscillations can be understood by a simple interferometer model [4] (Figure 1, top). Reflection of electrons at the interfaces builds up standing waves whenever the round-trip phase is a multiple of 2π . The resulting interference fringes appear with a period of $\lambda/2$, where λ is the wavelength of the electrons. Thus, we are measuring the wavelength of electrons directly in real space, using the world's smallest interferometers. In the case of Cu(100) at $E=E_{\rm F}$ and ${\bf k}^{\parallel}=0$, we obtain a wavelength of 2 nm. It might be puzzling why this value is so much larger than the Fermi wavelength, which is comparable to a lattice constant. What is measured here is the wavelength of an envelope function that modulates the normal Bloch function in order to satisfy the boundary conditions at the interfaces [2].

To see the connection between density of states and quantum well states [2], we have to look at the whole spectrum of electronic states (Figure 2). For a bulk Cu(100) crystal (top spectrum), a continuous spectrum is observed which corresponds to the s, p band with Δ_1 symmetry that straddles the Fermi level and has an upper cutoff at 1.8 eV above $E_{\rm F}$, which corresponds to the p_{λ} -like X'_{λ} point of the Cu band structure. In the thin-film spectra, which were obtained from overlayers differing in Cu thickness by two layers from one curve to the next, the continuous spectrum breaks up into discrete quantum well states. These states change their energy with decreasing Cu thickness and cross the Fermi level at regular thickness intervals. These Fermi-level crossings give rise to the density-of-states maxima in Figure 1. The fact that quantum well states change their energy with thickness is easy to understand by electron counting. In a finite slab of N atomic layers, one has N states at each \mathbf{k}^{\parallel} point. Therefore, the energy interval between adjacent states shrinks as 1/N with increasing film thickness and approaches zero for the bulk. For the very thin films in Figure 2, the spacings are still large compared to kT =0.026 eV (at room temperature): e.g., five unoccupied states within 2 eV for a 20-monolayer film, giving an average spacing of 0.4 eV. We would have to make the films 15 times thicker (about 50 nm) to reach the point at which the energy spacing becomes comparable to kT. Again, these dimensions place the region of interest in the nanometer regime.

Oscillatory magnetic coupling and GMR

The quantum well states seen in Figures 1 and 2 are closely correlated with magnetic properties such as oscillatory magnetic coupling and giant magnetoresistance (GMR). Figure 3 compares the density of states [2], spinpolarization [5], and magnetic coupling [6] for the fcc Cu/Co(100) system. All three quantities are found to oscillate with the same period of about six atomic layers (1 nm). Giant magnetoresistance in trilayers [7] exhibits the same period, since it is tied to antiparallel coupling. Such an agreement is found wherever comparable data exist [1, 2], e.g., for Ag/bcc Fe(100), Au/bcc Fe(100), Cu/fcc Co(100), and Cu/fcc Fe(100). For the short-period oscillations in Cu/fcc Co(100), observation of this effect requires highly perfect interfaces [8]. Recently, density-ofstates oscillations have also been seen for transition-metal spacers [9]: i.e., Cr/bcc Fe(100). After seeing such a correlation in periodicities, one would like to make the physical connection between quantum well states and oscillatory magnetic coupling. This can be done by calculating the total energy of all occupied quantum well states and observing it jump periodically with increasing thickness whenever a new state crosses the Fermi level [10]. Here we restrict ourselves to a qualitative discussion,





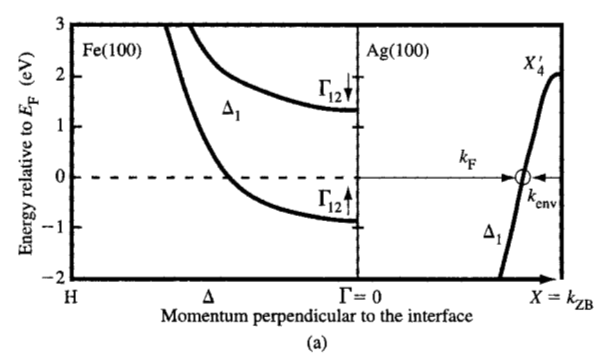
Inverse photoemission spectra for Cu films of varying thickness on fcc Fe(100). The s, p-band continuum of bulk Cu (top spectrum) splits into discrete quantum well states (numbered). From [2], reproduced with permission.

using a suggestion that explains why antiparallel coupling correlates with a density-of-states maximum at the Fermi level $E_{\rm F}$ in Figure 3. A high density of states at $E_{\rm F}$ is energetically unfavorable. Thus, the magnetic arrangement will undergo a restructuring to minimize the density of states at $E_{\rm F}$. In a trilayer, confined quantum well states can occur only for parallel orientation of the magnetic layers [11], as shown in **Figure 4(a)**. For an antiparallel orientation, the wave functions extend into one of the magnetic layers. Therefore, a transition to antiparallel

Comparison of oscillations in density of states (a), spin-polarization (b), and magnetic coupling (c) for fcc Cu/Co(100) sandwich structures. Identical periods of six monolayers (ML) are observed, suggesting a connection between quantum well states at the Fermi level and oscillatory magnetic coupling. The magnetoresistance of trilayer structures also oscillates with the same period [7] (not shown), since it requires antiparallel coupling. Part (a) from [2], part (b) from [5], part (c) from [6], reproduced with permission.

coupling circumvents the high density of states created by a quantum well state. Following this argument, it might be puzzling that quantum well states are observed in Figures 2 and 3 for spacer thicknesses characteristic of antiparallel coupling. The density-of-states data are not for trilayers, however, but for Cu/Co(100) bilayers, where one of the ferromagnetic layers is replaced by vacuum, which always confines the wave function. It is difficult to perform such

¹ S. D. Bader, Argonne National Laboratory, private communication.



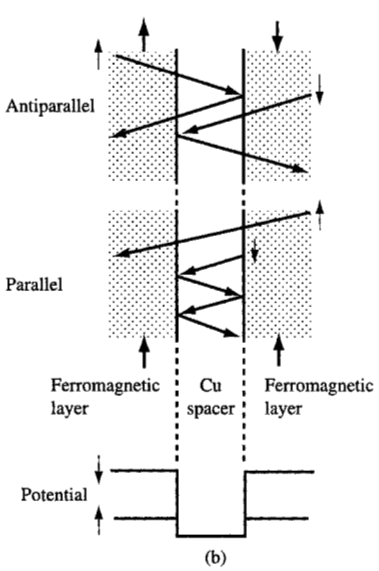


Figure 4

(a) Connection between the spin-polarization of quantum well states and spin-dependent reflectivity. Minority spin states cannot propagate from fcc Ag(100) into bcc Fe(100) at the Fermi level $E_{\rm F}$, since there are no minority states with the same Δ_1 symmetry in Fe(100). Instead, they form standing waves, i.e., discrete quantum well states. Majority spin states are able to propagate and remain a band-like continuum. From [2], reproduced with permission. (b) Schematic of the possible wave functions in trilayers, where two ferromagnetic layers are separated by a nonmagnetic Cu spacer. Quantized states exist only for parallel magnetization (bottom), or in a bilayer, where one of the ferromagnetic layers is replaced by vacuum.

surface-sensitive experiments for trilayers, where the ferromagnetic overlayer tends to swamp the signal from the spacer. First results on trilayers demonstrate that it is possible to penetrate the overlayer under favorable conditions [11].

Quantum well states must be spin-polarized for transmitting magnetic information, even in a noble-metal spacer such as Cu. This rather counterintuitive picture of a "magnetized" noble metal has been confirmed by spinpolarized photoemission [5, 12] (Figure 3, middle) and by magnetic circular dichroism [13]. There is a rather simple and general explanation for the spin-polarization of quantum well states in magnetic multilayers. Since they are formed by reflection of electrons at the interfaces, any spin-dependence in the reflectivity affects their confinement. In particular, the reflectivity at a ferromagnet differs between majority and minority spins, because of the magnetic exchange splitting of the bands. A particularly clear-cut case [2] is shown in Figure 4(b) for the interface between fcc Ag(100) and bcc Fe(100) at $\mathbf{k}^{\parallel} = 0$. Minority spin states at $E_{\rm p}$ in the Ag layer have no counterpart in Fe. Therefore, they are totally Braggreflected. Majority states, on the other hand, exist on both sides of the interface and are able to propagate. This leads to quantum well states with minority spin character, which have been observed by spin-polarized photoemission [12]. They are superimposed on a continuum of majority spin states. In general, there is not such a clear distinction between the reflectivity of majority and minority spins. However, one can argue that there will always be a spindependent potential step at the interface that makes the reflectivity spin-dependent [10]. For spacer layers to the right of the ferromagnets in the periodic table, the majority bands are more closely aligned than the minority bands because of a better match in band filling. This explains the observation of quantum well states with minority spin in noble metals. For spacers to the left of the ferromagnets, e.g., Cr, the situation is reversed, and one expects quantum well states with majority spin character. There are indications of quantum well states in Cr, but their spin-polarization has not yet been measured [9, 14]. This argument holds independently of the specific band topology, but it does not guarantee full confinement, which would require 100% reflectivity at the interface.

Spin-dependent reflectivity of electrons at interfaces is not only important for quantum well states and magnetic coupling, but might have an effect on giant magnetoresistance [15] as well. Models of the magnetoresistance for "conductivity in-plane" (CIP) and "conductivity perpendicular to the plane" (CPP) provide spin asymmetries for interface and bulk scattering in magnetic multilayers. Typically, interface spin asymmetries are four times larger than in the bulk, which leads to the fact that the CPP geometry exhibits 3-10 times higher magnetoresistance than the CIP configuration [16]. It should be kept in mind, though, that these asymmetries could be due to diffuse scattering instead of the specular reflection discussed here, and that many other parameters enter into the equations for magnetoresistance [15]. Concentrating on specular interface scattering in the CPP geometry, one can construct a simple polarizer-analyzer model for giant magnetoresistance: Each interface with a

ferromagnet acts as a polarization filter for electrons. If two magnetic layers are aligned antiparallel, one has the analog of crossed optical polarization filters, i.e., little transmission. If they are parallel, they both transmit electrons. The smaller magnetoresistance of the CIP geometry can be understood as a shunting effect whereby electrons are able to avoid spin-dependent scattering at the interfaces by traveling inside the layers. In order to achieve the high magnetoresistance of the CPP geometry but avoid its extremely low absolute resistance ($\mu\Omega$ and less), several attempts have been made to produce onedimensional wire or thin-film stripe structures, in which the current runs perpendicular to the interfaces but is confined to the wire or the thin film of stripes. Lithographic patterning has been used to produce sawtooth-shaped Si substrates for the deposition of magnetic stripes [17]. Magnetic wires perpendicular to the surface have been obtained by filling pores in a polymer film with electroplated metals [18]. Designing such structures opens up a fascinating world of low-dimensional growth phenomena. In the following section, we discuss a new approach for producing stripes with nanometer width at stepped surfaces.

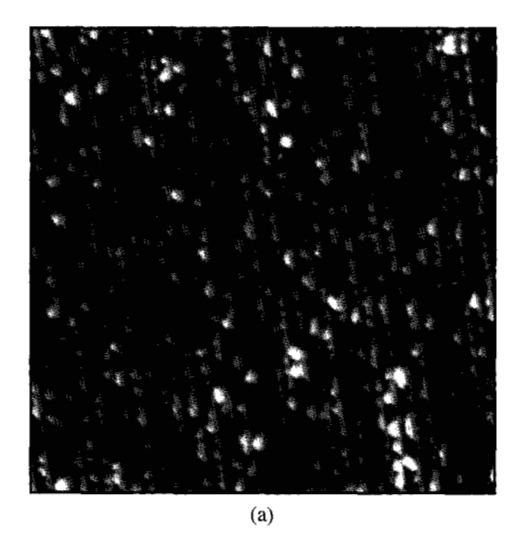
Since electron reflectivity at interfaces plays an important role in the magnetic phenomena discussed here, it is natural to try modifying the phenomena by coating the interfaces with a different material. Using one or two monolayers of a ferromagnet with large magnetic band splitting, such as Co, it has been possible to enhance the magnetoresistance of permalloy/Cu/permalloy structures by more than a factor of 2 [19]. A variety of special electronic states have been found at such "doped" interfaces by inverse photoemission [20], e.g. in Cu/Co/Ni(100). A Co3d-like interface state builds up at the same fast rate as the enhanced magnetoresistance, suggesting a connection with the magnetic band splitting in Co, which is three to four times as large as in Ni. (The spin splitting [1] is about 2 eV in bcc Fe, 1 eV in fcc Fe, 1 eV in fcc and hcp Co, and 0.3 eV in fcc Ni.) Quantum well states in the subsequent Cu layer are enhanced near the interface, indicating stronger confinement by higher, spin-dependent reflectivity. Going to thicker ferromagnetic overlayers, one finds quantum well states not only in the noble-metal spacer, but also in the ferromagnet [4, 20]. Returning to the optical interferometer analogy, one now has reflective or antireflective coatings on the electron mirrors, and the reflectivity oscillates with the thickness of the ferromagnetic overlayer. This affects the strength of the magnetic coupling, but not its periodicity, which is determined by the noble-metal spacer layer [10].

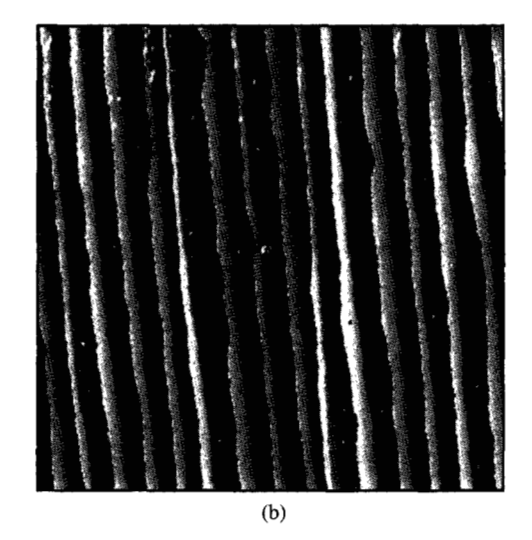
Stripes and dots at stepped surfaces

For growing one-dimensional nanostructures we consider growth at stepped surfaces, where the steps provide a template for attaching magnetic wires or stripes [21]. In the two-dimensional world of the first monolayer growing on a stepped surface, one can observe growth modes analogous to laver-by-laver and Stranski-Krastanov growth in three dimensions. As shown in Figure 5, Cu grows on a stepped Mo(110) surface in parallel stripes that correspond to a row-by-row growth mode [21]. On W(110), however, only the first row of Cu atoms decorates the step edge [22], and additional Cu grows in monolayerheight islands that are attached to the step edges [23], analogous to Stranski-Krastanov growth. An additional phenomenon at stepped surfaces is the presence of an energy barrier for crossing steps. This is obvious for an uphill crossing, since the atom incorporated at the step edge would be less coordinated on the terrace. Even for a downhill crossing, the atom must temporarily give up neighbors when crossing the step edge. An atom exchange mechanism can eliminate this barrier on certain metals during homoepitaxy [24]. In a heteroepitaxial system, such as Cu/Mo(110), the Cu atom crossing a Mo/Cu boundary trades Mo neighbors for Cu neighbors, which provide less binding energy. Such a barrier causes the inhomogeneous width of the Cu stripes on Mo(110) in Figure 5(b). The wider the terrace on which a Cu stripe resides, the wider the stripe. Apparently, the Cu atoms migrate toward the uphill edge of an individual terrace. It requires higher annealing temperatures to let Cu atoms cross step edges and equilibrate their stripe width, independent of the terrace width. Stripes with a uniform width of 3 nm have been obtained [21] for Cu on stepped Mo(110) after annealing to 600°C. The existence of uniform stripes in spite of nonuniform terraces indicates that the binding energy of Cu increases monotonically toward the step edge.

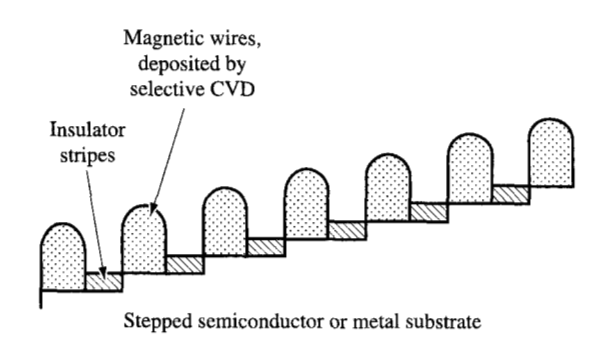
To make step decoration a widely applicable technique, it has been proposed that a two-step process be used [21] (Figure 6): In the first step, a template of inert stripes is grown by step flow. In the second step, the desired material is deposited selectively on the remaining stripes of the reactive substrate using chemical vapor deposition (CVD). For example, one could consider a stepped Si(111) surface as substrate, grow passivating stripes of lattice-matched CaF, along the step edges, and deposit metals by selective CVD on the remaining Si. Compounds for substrate-selective CVD have been developed for contacting Si devices through via holes in SiO, without shorting out the SiO, insulation. Selective deposition of W or Ta via WF, or TaF, might be useful to create a reaction barrier on the Si stripes against the formation of silicides with Fe, Co, or Ni. For the deposition of noblemetal spacers, such as Au, there exist organometallic precursors [25]. The spacers could also be simply evaporated after selective CVD of ferromagnetic wires.

If it becomes feasible to grow magnetic nanowires by step decoration, one could go one step further and





Observation of two different growth modes in two dimensions. Cu grown on stepped W(110) (a) and Mo(110) (b) respectively displays the analog of Stranski-Krastanov and layer-by-layer growth. The average step spacing is 50 nm. From [21], reproduced with permission.



Firefra 6

Illustration of a proposed "universal" deposition method for producing striped structures on a stepped surface. Initially, a set of inert stripes, e.g., an insulator, is deposited by step-flow growth. These act as templates for selective deposition of the magnetic wires on the remaining substrate. From [21], reproduced with permission.

produce an array of regular dots by patterning the wires lithographically (**Figure 7**). Using a UV laser, a standing-wave pattern with a periodicity of 200 nm can be produced on a photoresist that would allow elongated dots with typical dimensions of $20 \times 200 \text{ nm}^2$. Such a regular array of highly anisotropic magnetic particles might make

a good medium for the ultimate goal in magnetic recording, single-particle-per-bit storage [26-28]. Current media with randomly segregated particles in a CoPtCr alloy typically use 10³ particles per bit to reduce the readout noise introduced by irregular particles and domains. Working with a small subarray of magnetic dots per bit (say 1×100) already reduces this large number significantly without deviating too far from the traditional longitudinal recording geometry. When the number of dots per bit becomes too small, however, one is likely to run into tracking problems. Other geometries are conceivable that preserve a reasonably wide track, e.g., the two-particle-per-bit transverse recording scheme shown in Figure 7. The stray field between antiparallel-magnetized pairs of elongated dots would become the readout signal. The two bit levels would correspond to magnetizations pointing toward each other or away from each other.

Element-sensitive STM via resonant tunneling

For determining how stripes grow at steps, it is essential to have a high-resolution microscope that not only resolves the topography but is also able to distinguish between the substrate and the new material incorporated at the step edges. For perfect step-flow growth of lattice-matched materials, there is no topographic contrast. To achieve chemical contrast, we have developed an element-specific version [29] of scanning tunneling microscopy (STM). It is based on resonant tunneling into empty

Lithographically defined breaks

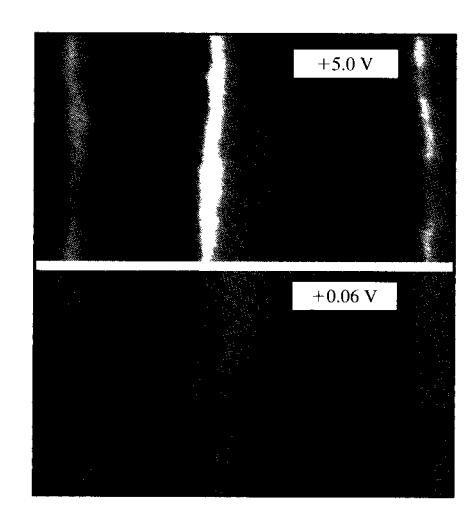
	↓	Magnetic wires along steps <				
Longitudinal						
V+ A/+/Y	*/4/-/4					
A/ + / +/ +/	V4 #/4 F/					
V + / + / + / + / + / + / - \frac{1}{2}	*/4*/4					
A/+ A/+	14 F/4 F/					
/*/*/*/	*/4 F/4 X	V////// V//////				
A/ # /4/ # /	V4 X-14 X-1					
0	1					
Transverse						
Y / / / / / / /	F/4/4/	V////// V//////				
14/4/2/4/	7/2/4/2/4/1	Y////// 1//////				

	Transverse			
0	(*/ Y / Y / Y)	F/4/4/	VIIIIA	//////
1	14/4/4/	() /) /) /) /		1//////
	<i>Y/////</i>		V/////	V/////
	1/////	V//////		7/////
	1/////	7/////	V/////	V//////
	7/////	V//////	7/////	1//////

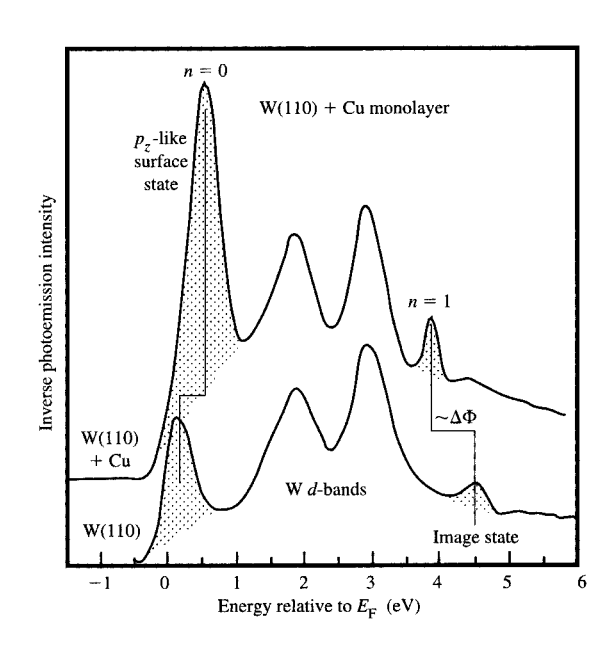
Proposed array of anisotropic magnetic dots produced by patterning a set of stripes lithographically (typical size $20 \times 200~\text{nm}^2$). Such a structure might be useful as a storage medium with uniform particle size. Blocks of these dots could be used for the usual longitudinal recording; pairs of dots could be used in a transverse recording scheme.

surface states that are specific to each metal. Thus, the electronic structure of nanostructures again becomes important. Figure 8 shows two STM images of the same three Cu stripes (about 3 nm wide) on a stepped Mo(110) surface. At specific bias voltages, it is possible to make the Cu appear either brighter than Mo (at +5 V) or darker (at +0.06 V). Such chemical contrast results from resonant tunneling of electrons from the tip into unoccupied surface states of the Cu or Mo, respectively. With most other bias voltages there is little contrast between the Cu and Mo (not shown). This reflects the topography, since Cu has practically the same size as Mo and grows in registry with the substrate lattice.

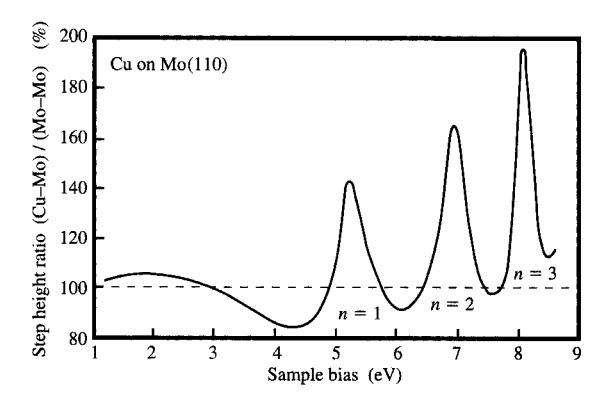
The states available for resonant tunneling can be found with inverse photoemission [23] (Figure 9, shaded states). There are two types of element-specific surface states for Cu on W(110) and Mo(110). One is a p_{\star} -like surface state near the Fermi level, the other an image state near the vacuum level. Mo appears bright at a bias of +0.06 V because of tunneling into its p_i-like surface state; Cu appears bright in Figure 8 at +5 V bias because of tunneling into its image state. While the upward shift of the p_{\cdot} -like surface state from W to Cu is nontrivial, the downward shift of the image state is easily understood. It tracks the work function reduction $\Delta\Phi$ from W to Cu, since image states are bound to the vacuum level E_{\perp} and the energy zero is the Fermi level $E_{\scriptscriptstyle \rm F}$ in inverse photoemission and STM ($\Phi = E_v - E_F$). The work functions of metal surfaces are well known and have been



STM images of 3-nm-wide Cu stripes on stepped Mo(110) with a step spacing of about 50 nm. Specific sample bias voltages can be used to enhance the brightness of either the Cu or Mo via resonant tunneling into surface states and image states (see Figure 9). From [29], reproduced with permission.



Inverse photoemission spectra from surface and image states of clean W(110) and from a Cu monolayer on W(110). Resonant tunneling into the shaded states provides contrast between the Cu and W in STM and allows their identification. From [22], reproduced with permission.



Finance 10

Resonant tunneling via image states for Cu stripes on stepped Mo(110). The apparent step height from a Mo terrace to a Cu step is plotted versus sample bias voltage. Enhancements of up to 100% are seen at the n=1,2,3 image-state resonances.

tabulated [30], allowing straightforward identification of different metals at a surface. Such tunneling resonances into image states are being modeled with realistic tip geometries [31].

To quantify resonant tunneling, we display the enhancement of the Cu stripes in the constant-current mode in Figure 10. The apparent height of the Mo-Cu step is normalized to the actual, Mo-Mo step height of 0.2 nm. At bias voltages corresponding to the n = 1, 2, 3image-state resonances, we find sharp resonances with enhancements of up to 100%. If we note that the tunneling current increases typically by two orders of magnitude over such a distance in STM, we expect a huge effect on current images at constant height. This large enhancement is due to the narrow intrinsic width of the image states, which can be as low as 0.02 eV in Cu. The p,-like surface state is broader and generally does not produce such a large effect, but it allows higher spatial resolution, since the tip comes closer to the surface at low bias voltages. For example, the narrow parts of the Cu stripes in Figure 8 are resolved in the high-resolution image at +0.06 V but are lost at +5-V bias. We have found it useful to first identify the low-work-function material by its n = 1 image state and then, by tuning to a low-bias surface state, proceed to a higher resolution.

Outlook

This brief overview has illustrated the key role played by electronic states in magnetic nanostructures. The states are connected with interesting effects observed in these structures, such as oscillatory magnetic coupling, giant magnetoresistance, and interface doping. They are also

essential for imaging the growth of nanostructures by resonant tunneling, e.g., imaging the growth of metallic stripes at stepped surfaces. The experiments with such self-assembled, one-dimensional structures are typical for a new wave of "engineered" materials. Magnetic and transport properties can be altered dramatically by structuring materials on a scale comparable to the electron wavelength, as demonstrated by noble-metal layers that become magnetized when sandwiched between ferromagnets. There is ample flexibility for designing magnetic structures that are customized for applications such as magnetic storage media or sensors.

Acknowledgment

This work was supported by the National Science Foundation under award numbers DMR-9624753 and DMR-9632527.

References

- 1. F. J. Himpsel, J. E. Ortega, G. J. Mankey, and R. F. Willis, Adv. Phys., in press.
- J. E. Ortega and F. J. Himpsel, Phys. Rev. Lett. 69, 844 (1992);
 J. E. Ortega, F. J. Himpsel, G. J. Mankey, and R. F. Willis, Phys. Rev. B 47, 1540 (1993) and J. Appl. Phys. 73, 5771 (1993).
- 3. J. E. Ortega and F. J. Himpsel, *Appl. Phys. Lett.* **64**, 121 (1994).
- 4. F. J. Himpsel, Phys. Rev. B 44, 5966 (1991).
- 5. C. Carbone, E. Vescovo, O. Rader, W. Gudat, and W. Eberhardt, *Phys. Rev. Lett.* **71**, 2805 (1993).
- Z. Q. Qiu, J. Pearson, and S. D. Bader, *Phys. Rev. B* 46, 8659 (1992).
- S. S. P. Parkin, R. Bhadra, and K. P. Roche, *Phys. Rev. Lett.* **66**, 2152 (1991); F. Petroff, A. Barthélemy, D. H. Mosca, D. K. Lottis, A. Fert, P. A. Schroeder, W. P. Pratt, R. Loloee, and S. Lequien, *Phys. Rev. B* **44**, 5355 (1991); X. Bian, H. T. Hardner, and S. S. P. Parkin, *J. Appl. Phys.* **79**, 4980 (1996).
- 8. P. Segovia, E. G. Michel, and J. E. Ortega, *Phys. Rev. Lett.* 77, 3455 (1996).
- 9. Dongqi Li, J. Pearson, S. D. Bader, E. Vescovo, D.-J. Huang, P. D. Johnson, and B. Heinrich, *Phys. Rev. Lett.* 78, 1154 (1997).
- D. M. Edwards, J. Mathon, R. B. Muniz, and M. S. Phan, *Phys. Rev. Lett.* 67, 493 (1991) and *J. Phys. Condens. Matter* 3, 4941 (1991); M. D. Stiles, *Phys. Rev. B* 48, 7238 (1993); B. A. Jones and C. B. Hanna, *Phys. Rev. Lett.* 71, 4253 (1993); P. Bruno, *Phys. Rev. B* 52, 411 (1995); see also B. A. Jones, *IBM J. Res. Develop.* 42, 25 (1998, this issue).
- 11. F. J. Himpsel and O. Rader, Appl. Phys. Lett. 67, 1151 (1995).
- 12. N. B. Brookes, Y. Chang, and P. D. Johnson, *Phys. Rev. Lett.* **67**, 354 (1991).
- M. G. Samant, J. Stöhr, S. S. P. Parkin, G. A. Held, B. D. Hermsmeier, F. Herman, M. van Schilfgaarde, L.-C. Duda, D. C. Mancini, N. Wassdahl, and R. Nakajima, *Phys. Rev. Lett.* 72, 1112 (1994); S. Pizzini, C. Giorgetti, A. Fontaine, E. Dartyge, G. Krill, J. F. Bobo, and M. Piecuch, *Phys. Rev. Lett.* 74, 1470 (1995); See also J. Stöhr and R. Nakajima, *IBM J. Res. Develop.* 42, 73 (1998, this issue).
- 14. J. E. Ortega, F. J. Himpsel, G. J. Mankey, and R. F. Willis, *Mater. Res. Soc. Symp. Proc.* **313**, 143 (1993).
- 15. For an overview of GMR, see R. K. Nesbet, *IBM J. Res. Develop.* 42, 53 (1998, this issue).

- W. P. Pratt, S.-F. Lee, J. M. Slaughter, R. Loloee, P. A. Schroeder, and J. Bass, *Phys. Rev. Lett.* 66, 3060 (1991);
 W. P. Pratt, S.-F. Lee, Q. Yang, P. Holody, R. Loloee, P. A. Schroeder, and J. Bass, *J. Appl. Phys.* 73, 5326 (1993).
- T. Ono and T. Shinjo, J. Phys. Soc. Jpn. 64, 363 (1995);
 M. A. M. Gijs, M. T. Johnson, A. Reinders, P. E.
 Huisman, R. J. M. van der Veerdonk, S. K. J. Lenczowski, and R. M. J. van Gansewinkel, Appl. Phys. Lett. 66, 1839 (1995);
 W. Oepts, M. A. M. Gijs, A. Reinders, R. M. Jungblut, R. M. J. van Gansewinkel, and W. J. M. de Jonge, Phys. Rev. B 53, 14,024 (1996).
- L. Piraux, J. M. George, J. F. Despres, C. Leroy, E. Ferain, R. Legras, K. Ounadjela, and A. Fert, Appl. Phys. Lett. 65, 2484 (1994); A. Blondel, J. P. Meier, B. Doudin, and J.-Ph. Ansermet, Appl. Phys. Lett. 65, 3019 (1994); K. Liu, K. Nagodawithana, P. C. Searson, and C. L. Chien, Phys. Rev. B 51, 7381 (1995).
- S. S. P. Parkin, Appl. Phys. Lett. 61, 1358 (1992) and Phys. Rev. Lett. 71, 1641 (1993).
- C. Hwang and F. J. Himpsel, *Phys. Rev. B* 52, 15,368 (1995).
- F. J. Himpsel, Y. W. Mo, T. Jung, J. E. Ortega, G. J. Mankey, and R. F. Willis, Superlattices & Microstructures 15, 237 (1994); T. Jung, R. Schlittler, J. K. Gimzewski, and F. J. Himpsel, Appl. Phys. A 61, 467 (1995).
- 22. F. J. Himpsel and J. E. Ortega, *Phys. Rev. B* **50**, 4992 (1994).
- Y. W. Mo and F. J. Himpsel, *Phys. Rev. B* 50, 7868 (1994).
- R. Stumpf and M. Scheffler, *Phys. Rev. Lett.* 72, 254 (1994).
- M. M. Banaszak Holl, P. F. Seidler, S. P. Kowalczyk, and F. R. McFeely, *Appl. Phys. Lett.* 59, 324 (1991) and *Inorgan. Chem.* 33, 510 (1994).
- R. M. H. New, R. F. W. Pease, and R. L. White, J. Vac. Sci. Technol. B 12, 3916 and 13, 1089 (1995).
- S. Y. Chou, P. R. Krauss, and L. Kong, J. Appl. Phys. 79, 6101 (1996).
- M. Hehn, K. Ounadjela, J.-P. Bucher, F. Rosseaux, D. Decanini, B. Bartelian, and C. Chappert, *Science* 272, 1782 (1996).
- 29. T. Jung, Y. W. Mo, and F. J. Himpsel, Phys. Rev. Lett. 74, 1641 (1995); for a review on chemical sensitivity in STM, see T. Jung, F. J. Himpsel, R. Schlittler, and J. K. Gimzewski, Chemical Information from Scanning Probe Microscopy and Spectroscopy, in STM IV—Analytical SXM Techniques, R. Wiesendanger, Ed., Springer Series in Surface Science, in press.
- J. Hölzl and F. K. Schulte, Work Function of Metals, Springer Tracts in Modern Physics 85, Springer-Verlag, Berlin, 1979, p. 1.
- 31. T. M. Kalotas, A. R. Lee, J. Liesegang, and A. Alexopoulos, Appl. Phys. Lett. 69, 1710 (1996).

Received November 7, 1996; accepted for publication April 21, 1997

Franz J. Himpsel Department of Physics. University of Wisconsin, Madison, Wisconsin 53706 (himpsel@comb.physics. wisc.edu). Professor Himpsel received a Ph.D. degree from the University of Munich in 1976; his thesis was based on early angle-resolved photoemission experiments using synchrotron radiation. He joined D. E. Eastman's group at the IBM Thomas J. Watson Research Center in 1977 as a Postdoctoral Fellow and became a Research Staff Member in 1980, a manager in 1982, and a senior manager in 1985, heading the Research Center's Surface Physics Department. Since the fall of 1995 he has been a member of the Physics Department of the University of Wisconsin at Madison, and since 1996 has been the Associate Director for Research at their Synchrotron Research Center. Professor Himpsel's work has covered the areas of surface physics studies using synchrotron radiation, the electronic structure of semiconductor surfaces using core-level spectroscopy, angleresolved photoemission and inverse photoemission, and the mapping of energy-band dispersions. His current interests are focused on the "engineering" of surfaces on the atomic scale. He is a member of the American Physical Society, the American Vacuum Society, and the German Physical Society. Professor Himpsel received the Peter Mark Award of the American Vacuum Society in 1985. He has been a Fellow of the American Physical Society since 1985, a Fellow of the American Vacuum Society since 1994, and a member of the New York Academy of Sciences since 1995.

Thomas A. Jung Laboratory for Micro- and Nanostructures, Paul Scherrer Institute (PSI), CH-5232 Villigen PSI, Switzerland (Thomas.Jung@psi.ch). Dr. Jung is a Research Staff Member at the Paul Scherrer Institute, which is affiliated with the Swiss Federal Institute of Technology. His research activities are in the field of nanometer-scale science and technology. Dr. Jung joined the IBM Thomas J. Watson Research Laboratory as a Postdoctoral Fellow in 1992 to work on scanning tunneling microscopy and spectroscopy of metallic wires and islands. From 1994 to 1997, he explored interfaced molecular nanostructures, in the course of which molecular positioning was achieved for the first time at room temperature, and unique methods for the identification and analysis of the conformation of an individual molecule were demonstrated. Dr. Jung received a Diplom degree in physics from the Swiss Federal Institute of Technology in 1987 and a Ph.D. in solid-state and surface physics from the University of Basel, Switzerland, in 1992. Highlights of his Ph.D. work include the development of atomic force microscopy as a tool for surface structuring and tribological analysis and highsensitivity magnetic force microscopy that subsequently proved single-flux-line sensitivity. Before joining IBM, he worked on the implementation of atomic force microscopy in the research and development activities at the PSI Zurich (formerly RCA) Research Laboratory. Dr. Jung is a member of the American Physical Society and the Swiss Physical Society.

Paul F. Seidler IBM Research Division, Zurich Research Laboratory, Säumerstrasse 4, CH-8803 Rüschlikon, Switzerland (pfs@zurich.ibm.com). Dr. Seidler is Manager of Display Technology at the IBM Zurich Research Laboratory, where he and his group are currently developing devices based on organic light-emitting diodes. He received a B.S. in chemistry from the California Institute of Technology in 1980 and a Ph.D. in chemistry from the University of California at Berkeley in 1985. His thesis was in the field of mechanistic organometallic chemistry. Dr. Seidler subsequently joined the Exxon Corporation as a Postdoctoral Fellow at its Corporate Research facility, where he continued working until 1988 on fundamental chemical and physical studies aimed at the

activation of saturated hydrocarbons such as methane. He then moved to the IBM Thomas J. Watson Research Center as a Research Staff Member in the Physical Sciences Department. At IBM he has worked on a variety of scientific studies related to semiconductor processing technology, in particular the kinetics and mechanisms of metal chemical vapor deposition. He also served a year as Technical Assistant to the Vice President, Systems, Technology, and Science, for the IBM Research Division. Dr. Seidler assumed his present position in September 1995. He is a member of the American Chemical Society and Sigma Xi.